Direction-selective free expansion of laser-produced plasmas from planar targets

Th. Müller,[1] B. K. Sinha,[2] and K. P. Rohr[1]
[1]*Fachbereich Physik, Universität Kaiserslautern, D-67663 Kaiserslautern, Germany*
[2]*Laser and Plasma Technology Division, Bhabha Atomic Research Centre, Mumbai 400 085, India*
(Received 15 November 2002; published 26 February 2003)

Direction-selective expansion of laser-produced plasmas from planar slab targets of Al, Ni, Mo, and Ta are reported. Angular distributions of the particles emitted from the targets, produced by a 130 mJ, 5 nsec, Nd:YAG laser, were obtained by means of a retarding potential analyzer and a quartz crystal. It was observed that the angular distributions of the particles had mainly three characteristics. For a given laser energy and a given target element, the angular distribution showed more preferential focusing toward the target normal as the value of the focal spot size *B* increased. Second, for a given laser energy and a given focal spot size, the focusing was more pronounced toward the target normal as the atomic mass number of the target materials increased. Third, for a given energy, a given focal spot size and a given element, the particles with higher ionization states were much more focused toward the target normal. Our experimental results confirm the Monte Carlo simulation results of the earlier works taking into account collision and recombination processes.

DOI: 10.1103/PhysRevE.67.026415 PACS number(s): 52.38.Mf, 52.50.Jm, 81.15.Fg

I. INTRODUCTION

In the field of material preparation such as fabrication of thin films of high-T_c superconductors, oxides, semiconductors, and diamondlike carbon laser pulsed-deposition technique has been found to be interesting and useful [1–20]. The partition of energy as well as the angular distribution of the emitted materials have a great influence on the quality of the deposited layers [21]. Buttini, Thum-Jäger, and Rohr [17] and Thum-Jäger and Rohr [18] have shown that if the angular distributions are fitted in the usual way as a two-component structure by the superposition of a broad cosine and a steep $\cos^n$ function in the form of a $\cos\theta + b\cos^n\theta$ [19], with a and b being constants, and θ is the angle between target normal and the angle of observation, the most important feature is that the steep directed component increasingly dominates the emission with an increase in the atomic mass number A. Thum-Jäger and Rohr [18] gave an average scaling law for the exponent n, i.e., $n \propto A^{3/4}$ and was found to be in agreement with the experimental investigations by Müller and Rohr [20]. Müller and Rohr experimentally obtained the values of n as 18 and 50 for pure copper and tungsten, respectively, though they also investigated the value of n for copper and tungsten alloy which gave the value of n in between. These experimental investigations demonstrate that the free expansion of laser-produced plasmas from planar targets is direction selective and is directed essentially towards the normal to the target surface. However, it should be noted that the two-component fit is only a basis to discuss and compare the observed or calculated behavior [15]. It is not clear whether the two components $\cos\theta$ and $\cos^n\theta$ have any physical meanings by their own, including the weight factors a and b. The broad background structure might, in the recombination model [14], at least, in part, be due to recombining collisions, which has a physical meaning.

The causes for this direction-selective behavior of the freely expanding plasma are not well known, but a number of theoretical and experimental studies have reported the importance of gas-phase collisions in the formation of the forward peaked angular distributions of the particles described by the term $\cos^n\theta$. Kelly and Dreyfus [22,23] reported that about three collisions per particle suffice for the formation of a Knudsen layer resulting in an angular distribution with $n = 4$. With the number of collisions having a value of more than three, Kelly [24] used the unsteady adiabatic expansion to describe the flow. He reported that, in this case, the angular distribution was more focused towards the target normal with n having the values between 4.3 and 43 depending on the yield of the material per pulse. Additionally, from the numerical calculations based on the Monte Carlo simulation of the desorption process, Sibold and Urbassek [11] and Noor Batcha, Lucchese, and Zeiri [25] observed the focusing effect of gas-phase collisions. In their model, they considered the number of collisions to depend on two parameters: the number of monolayers ϑ desorbed per laser pulse, and the ratio $b = (r_o / V_T \tau)$, where r_o is the laser-spot size, V_T the thermal velocity at the surface, and τ the laser pulse duration. The expression $(V_T \tau)$ is a measure of the length of the gas cloud at the end of the desorption process. With $\vartheta = 2.5$ and $b = 5$, a value of $n = 17$ was obtained, though in real experiments, these parameters can be much higher.

Noor Batcha, Lucchese, and Zeiri [26] further reported the contribution of internal degrees of freedom into the kinetic energy of particles and its effect on the spread or defocusing of the angular distributions. Itina *et al.* [27] observed that the nonequilibrium chemical reactions in the gas phase during ablation affected the angular distributions in the way opposite to that of the elastic collisions. Itina, Marine, and Autric [28], in their subsequent works, presented the results of the Monte Carlo simulation of the laser desorption process. Besides elastic collisions, they also considered the recombination-dissociation process. They reported that, in the reactionless flow, the increase of b led to the increase of focusing of the angular distribution towards the target normal. This effect was attributed to the elastic collisions as the number of collisions was shown to increase with an increase in parameter b. Their simulations further showed that the

 ©2003 The American Physical Society

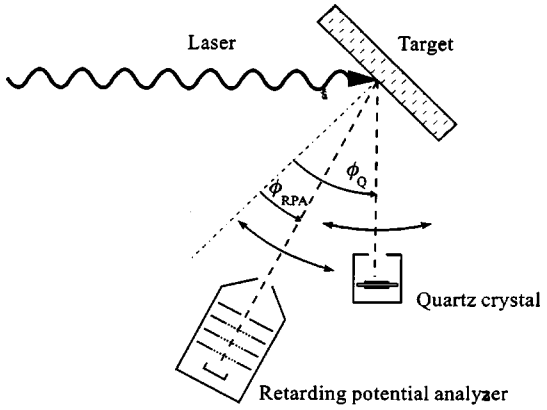

FIG. 1. Schematic diagram of the experimental setup. The laser pulse is incident at a fixed angle of 45°. Particle analysis is in the plane of incidence by a combination of a retarding potential analyzer and a quartz crystal.

chemical process gave rise to the broadening of the angular distributions and when *b* increases, the number of chemical reactions also increases, as well as that of elastic collisions. The focusing or defocusing of the angular distributions ultimately depends on the relative dominance of the two processes.

In the present work, we have investigated the direction-selective free expansion of laser-produced plasmas from the slab targets of Al, Ni, Mo, and Ta using a 130 mJ, 5 nsec, Nd:YAG laser. We report the experimental observation of the following results. For a given laser energy and the target material, the angular distribution showed more preferential focusing towards the target normal as the values of the focal spot size *B* increased. For the given laser energy and the given focal spot diameter, the focusing towards the target normal was more pronounced as the value of the atomic mass number increased. For a given laser energy, a given focal spot diameter and a given target element, the angular distribution showed more preferential focusing as the ionization state of the emitted particles increased. The results are well explained on the basis of the estimates of recombination and collision rates as well as on Monte Carlo simulations of earlier works [11,27,28]. Our results confirm the predictions of Monte Carlo simulations.

II. THE EXPERIMENT

A schematic representation of the experimental setup is displayed in Fig. 1. The plasma is created by an Nd:YAG laser ($E_L = 130$ mJ, $\tau = 5$ nsec, and $\lambda = 1.06$ μm) incident on planar targets at a fixed angle of $-45°$ with respect to the target normal. Target materials consisted of Al, Ni, Mo, and Ta. The particles of the freely expanding plasma were detected in an angular range relative to the target normal between $\phi_{\mathrm{RPA}} = 50°$ and $-10°$ for ions and $\phi_Q = 80°$ and $-15°$ for total number of particles by moving the analyzers within the plane of incidence, at a distance of 35 cm from the target.

The ion spectra were fully resolved by a combination of the time-of-flight and the retarding-potential method, which made it possible to obtain the absolute number of each species. The second detector consisted of an rf-excited quartz crystal. From the frequency change of the crystal after the plasma has been deposited, one obtains the total mass or, in the case of monatomic beams, the total number of particles. The number of the neutral particles could be deduced from the difference between the total particle signal and the summed spectra of the different ion species.

Some considerable efforts were invested in the laser and the detector systems to increase the reliability of the results.

(a) The shot-to-shot reproducibility of the laser was better than 3% and the incoming and back-reflected laser energies were monitored continuously.

(b) The ion detector was optimized concerning the surface effects at the apertures and secondary electron emission at the Faraday cup [20].

(c) The total particle measurements were multi-scaled up to 200-fold depending on the signal strength leading to a reproducibility better than 5%. The retarding potential spectra were multiscaled at least 20-fold for each setting of the retarding potential.

(d) Temperature effects, the sticking efficiency and the linearity of the frequency response of the crystal detector have been carefully tested in separate experiments. Details are given by Müller and Rohr [20].

We estimated that the overall uncertainty for the ion data in absolute particle numbers ranged between 10% and 40%, depending on the energies and charge states. Most of this uncertainty stemmed from the deconvolution procedure in the combined time-of-flight and retarding-potential method. The uncertainty for the total number of particles was estimated to be below 15%, whereby, the major contribution came from the integration over the half space.

III. EXPERIMENTAL RESULTS AND DISCUSSION

In Fig. 2 are displayed the integrally normalized angular distributions of the total number of particles of Al, Ni, Mo, and Ta as a function of the angle θ for three sizes of the focal spot ($B = 0.16$ mm^2, 0.94 mm^2, and 8.34 mm^2) at a laser energy of 130 mJ. We note that although all the distributions are focused towards the direction of the target normal, the focusing effect increases as the focal spot size increases. This also significantly increases with increase in the atomic mass number.

In Fig. 3, we have displayed charge-resolved integrally normalized distributions for two spot sizes $B = 0.61$ mm^2 and $B = 8.34$ mm^2 for the above mentioned four elements at the same laser energy. It is to be noted that the larger focal spot size has a stronger focusing effect. Further, as the ionization states of the ablated particles increase, the focusing towards the target normal is much more pronounced. In Fig. 4, we have displayed charge-resolved angular distributions of average ion velocity as a function of focal spot size for laser energy $E_L = 130$ mJ. It is to be noted that though the average ion velocities decrease with increase in mass, which is expected, the ions with higher value of charge have much larger values of average ion velocity for any given focal spot size. For spot sizes of 0.61, 1.44, 4.71, and 8.34 corresponding laser intensities are computed as 4.25×10^9, 1.8×10^9,

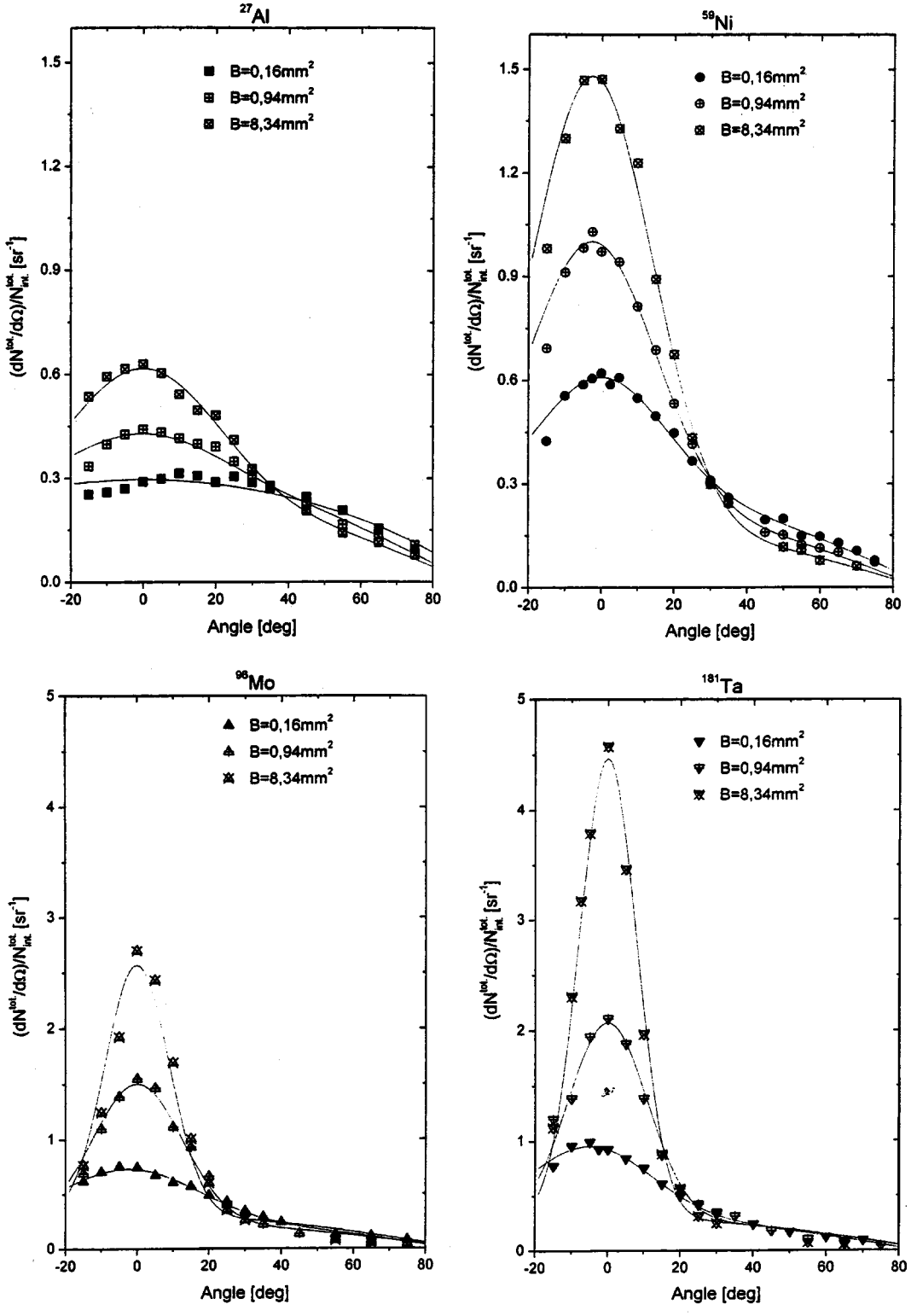

FIG. 2. Angular distribution of normalized integrated emissions from Al, Ni, Mo, and Ta for three focal spot sizes.

5.5×10^8, and 3.11×10^8 W/cm^2.

In Fig. 5(a), we have displayed the angular variation of average charge state for Al, Ni, Mo, and Ta at the same laser energy of $E_L=130$ mJ for only one value of $B=1.44$ mm^2 which corresponds to a laser intensity of 1.8×10^9 W/cm^2. In Fig. 5(b), maximum average charge state is displayed as a function of focal spot size for the given four materials. It is to be noted that the average charge state for any element significantly decreases as the angle increases, away from the target normal. From Fig. 5(b), we note that the maximum average charge state decreases as the focal spot size increases, i.e., the laser intensity decreases, which is expected.

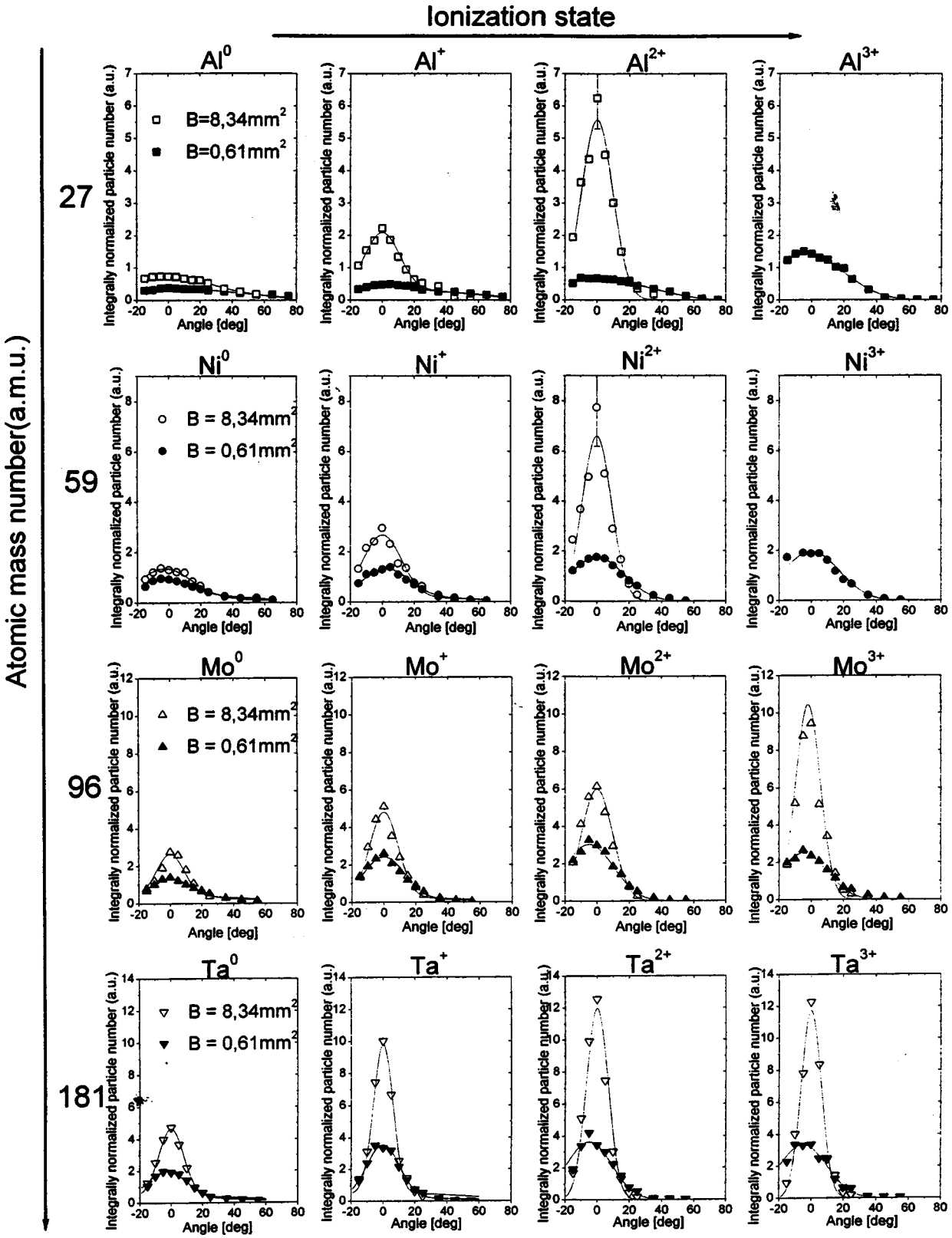

FIG. 3. Angular distribution of normalized integrated, charge-resolved particle emissions from Al, Ni, Mo, and Ta for two focal spot sizes.

But an important observation is that the maximum average charge state, for example for $B=0.61$ mm^2, significantly decreases with increasing mass number (charge number). Moreover, the figures of approximately 2.4, 1.9, 1.5, and 1.3 for Al, Ni, Mo, and Ta, respectively are much lower than the theoretical estimates of the charge states at the time of plasma formation, i.e., about 5 nsec which is the duration of the laser pulse. The scaling laws of plasma temperature for

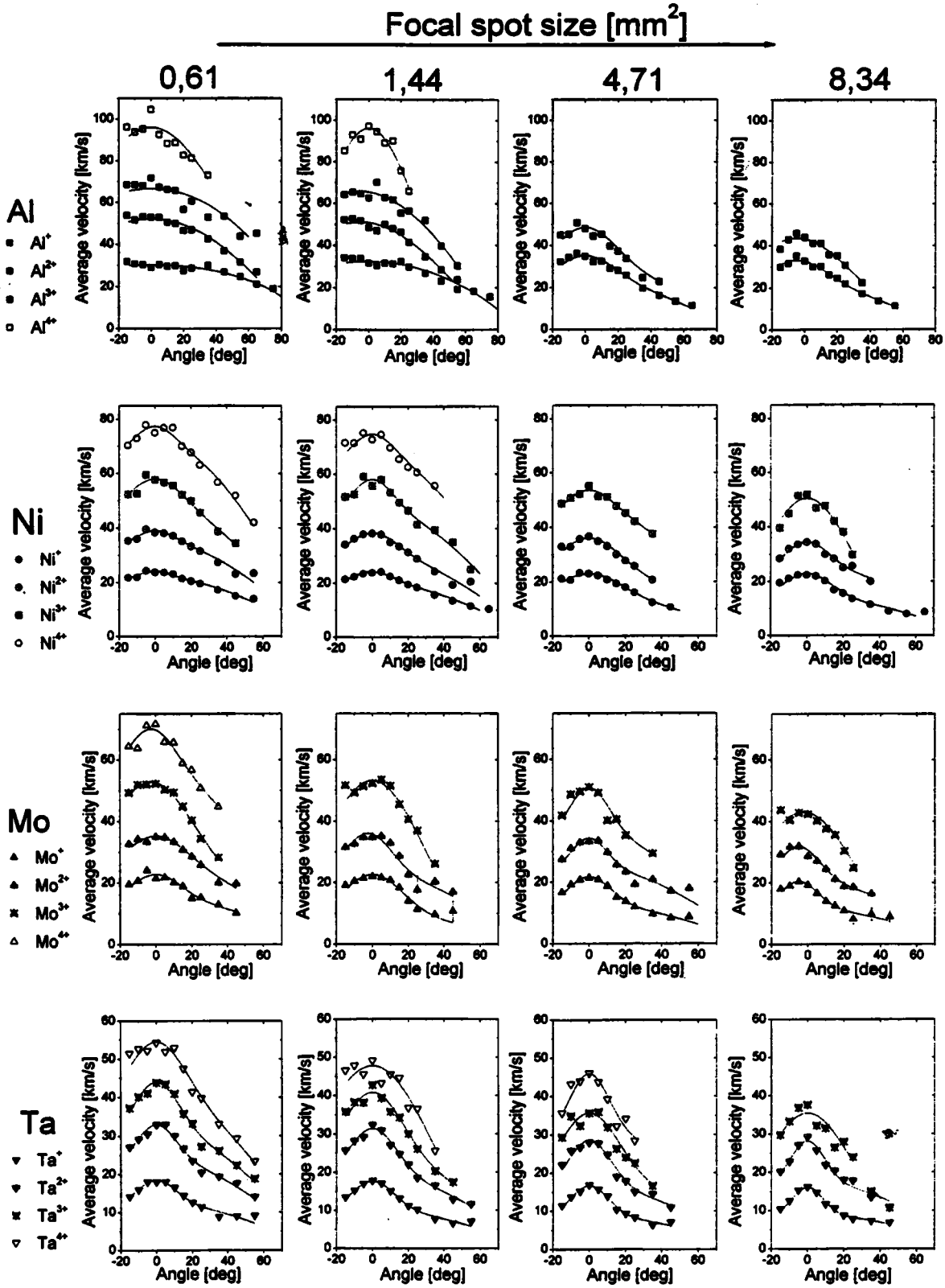

FIG. 4. Angular distribution of average charge-resolved ion velocities as a function of focal spot size (four focal spot sizes).

different target materials, as a function of laser intensity, have been variously reported by several authors [29–34]. It was reported that scaling laws were different for different target elements as well as they were different in different regimes of laser intensities. However, it was observed that the scaling laws were slower as the charge number Z of the target elements increased in the linear regime of laser-plasma interaction. From the measurements and scaling laws

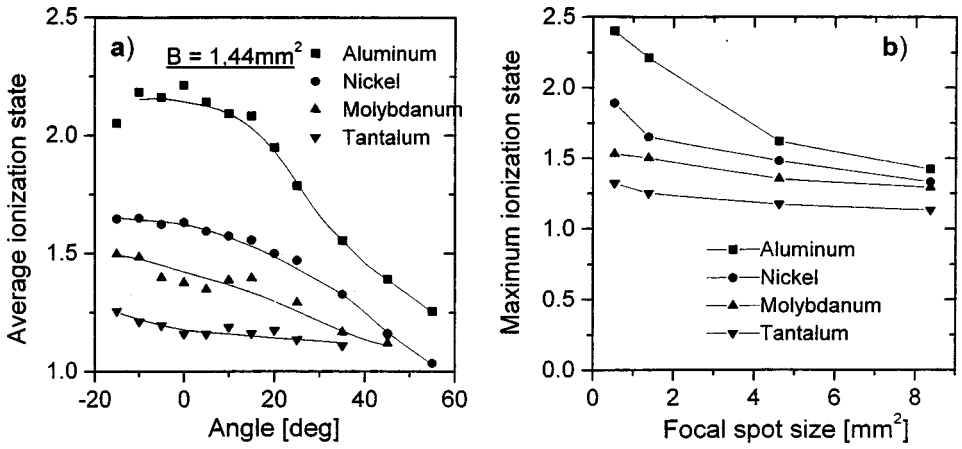

FIG. 5. (a) Angular distribution of average charge state for a fixed value of the focal spot size ($B=1.44$ mm^2, $I_L=1.8\times10^9$ W/cm^2) for Al, Ni, Mo, and Ta. (b) Maximum average charge state as a function of focal spot size for the same elements as in (a), $E_L=130$ mJ.

reported by Sinha and Gopi [30] for an Al plasma, the approximate electron temperatures for the elements considered in this paper have been estimated to be 71, 74, 80, and 85 eV for the four laser intensities of 3.1×10^8, 5.5×10^8, 1.8×10^9, and 4.25×10^9 W/cm^2, respectively.

To estimate the average ionization $\overline{Z}$ as a function of electron temperature, several authors [35–37] have given approximate relationship for high-Z plasmas, but the calculations of Mosher [37] seem to be more accurate. From Mosher's calculations, one can approximately estimate the values of $\overline{Z}$ at temperatures of 70 and 100 eV for Al ($Z=13$), Ni ($Z=28$), Mo ($Z=42$), and Ta ($Z=73$) as (9.5 and 11), (13.5 and 16), (14.5 and 17), and (20 and 22), respectively. It is to be noted that, for the temperatures under condition, the variation in $\overline{Z}$ is very small. For a temperature variation from 70 to 100 eV (a change of nearly 50%) $\overline{Z}$ varies approximately as $(15\pm1.5)\%$, $(18\pm1.8)\%$, $(17\pm1.7)\%$, and $(10\pm1.0)\%$. Now we come back to Fig. 2. It is to be noted that the focusing effect is much more pronounced for elements with higher atomic masses which also correspond to higher values of the charge number Z. For a given element, the focusing is stronger for higher focal spot size which corresponds to lower laser intensity. Itina and co-workers [27,28] used Monte Carlo simulation to study the role of chemical reactions, i.e., recombination and dissociation processes in addition to the gas-phase collisions, in the expansion dynamics of laser-ablated plasma particles. They observed that the angular distribution of atoms and ions and the angular distribution of their mean energies become less focused toward the surface normal if the number of recombination processes is sufficiently high. They further reported that, on the contrary, when the collision processes dominate, the ablated particles are more focused toward the target normal. Noor Batcha *et al.* [26] in their earlier work also reported the broadening (less focusing) of angular particle distribution due to nonequilibrium chemical reactions.

In the Monte Carlo simulation, it is possible to isolate the collisional and the recombination processes and to study, in detail, the effects of each one. However, in the experiments, it is not possible as both the processes occur simultaneously, and compete with each other. Therefore, it is useful to examine these processes, a bit, in detail. Among the three recombination processes, at the density ($\approx10^{18}$ cm^{-3}) and temperatures (70–85 eV) considered here, the contribution of dielectronic recombination can be ignored, which is significant only in the case of high temperatures and high densities [38,39]. With the help of a little algebra, it can be seen that radiative recombination varies as $\overline{Z}^2\mathrm{Te}^{-1/2}$ [40]. For three-body recombination, Zel'dovich and Raizer [41] have given an approximate relationship which varies as $\overline{Z}^3\mathrm{Te}^{-9/2}$. The electron-ion frequency (ν_{ei}), electron-electron collision frequency (ν_{ee}) and ion-ion collision frequency (ν_{ii}) vary approximately as $\overline{Z}\mathrm{Te}^{-3/2}$ and $\overline{Z}^4\mathrm{Ti}^{-3/2}$, respectively [42]. Kinetic ion temperatures for two representative focal spot sizes have been estimated by the technique reported by Thum-Jäger, Sinha, and Rohr [43] and are displayed in Table I.

Among the two recombination processes considered here, the three-body recombination is very dominant at temperatures and the density of the plasma reported in the present paper [39]. Hence, it will suffice to consider here the three-body recombination only. In Fig. 5(a), we have displayed the average ionization states for Al, Ni, Mo, and Ta as a function of the angle from the target normal for a fixed spot size. Figure 5(b) gives the maximum average ionization state as a function of the focal spot size and it is observed that the maximum occurs, for all the target materials, at an angle close to the target normal. Experimentally obtained maximum ionization states for Al, Ni, Mo, and Ta can be obtained approximately as 2.4, 1.9, 1.5, and 1.3, respectively. It should be noted that these values represent the average values of the ionization states after the recombination, in the core of the plasma, has taken place. The estimated values of the average ionization states from Mosher's calculations [37] are $\approx$11, 16, 17, and 22. This means that a strong recombination has taken place during the time interval of the laser pulse duration. But this is not enough. One has to know which processes, collision or recombination, are dominating, which seems, at this stage, a difficult question. When the focal spot size varies from $B=0.16$ mm^2 to $B=8.34$ mm^2 (Fig. 2), Te decreases from 85 to 71 eV, i.e., by a factor of 1.2 and the average decrease in the average ionization states, for all the four elements is also around a factor of 1.17. That is to say, the fractional decrease in Te and $\overline{Z}$ is nearly the same. From a simple calculation, one can see that because of this change in the plasma parameters, three-body recombination rate decreases by a factor of $\approx$1.3. The electron-ion collision fre-

TABLE I. Ion temperature for different ionization states of Al, Ni, Mo, and Ta as a function of two focal spot sizes. Laser energy $E_L = 130$ mJ, direction-target normal, i.e., $\theta = 0°$.

Ions	Focal spot B (mm^2)	Laser intensity (W/cm^2)	Kinetic ion temperatures (eV)
Al^{2+}	0.61	4.25×10^9	63.2
Al^{3+}			248.9
Al^{4+}			57.9
Al^{+}	8.34	3.11×10^8	6.1
Al^{2+}			51.5
Ni^{+}	0.61	4.25×10^9	101.4
Ni^{2+}			70.1
Ni^{3+}			40.4
Ni^{+}	8.34	3.11×10^8	78.3
Ni^{2+}			49.1
Ni^{3+}			8.9
Mo^{+}	0.61	4.25×10^9	52.2
Mo^{2+}			62.9
Mo^{3+}			16.3
Mo^{+}	8.34	3.11×10^8	40.0
Mo^{2+}			44.8
Mo^{3+}			24.5
Ta^{+}	0.61	4.25×10^9	61.6
Ta^{2+}			44.4
Ta^{+}	8.34	3.11×10^8	40.2
Ta^{2+}			21.7

quency ν_{ei} also increases by a factor of about 1.1. Hence, these two processes nearly neutralize each other. But when we consider the radiative recombination rate and the electron-electron collision frequency ν_{ee}, we find encouraging results. For the same amount of variation in the plasma parameters, the radiative recombination rate decreases by a factor of 1.31 and, at the same time, the electron-electron collision frequency also increases by a factor of 1.31. As a result, for larger values of the focal spot size, the focusing toward the target normal increases. These experimental results support the simulation results of Itina and co-workers [27,28].

In Fig. 2, we have further noted that for a given focal spot the focusing toward the target normal is much more pronounced as the atomic mass number of the target element increases. To explain this on the basis of recombination and collision rates, one needs more accurate measurements of temperatures for the given elements at different focal spot sizes. As these data are not available, we consider a second approach to explain the results. In their Monte Carlo simulations, Itina, Marine, and Autric [28] have considered a ratio $b = r_o/(V_T\tau)$ of the laser spot radius r_o to the length of the gas cloud at the end of the desorption process, where V_T is the thermal velocity at the surface temperature and τ is the laser pulse duration. They reported that the increase of b leads to the increase of focusing of the angular distribution toward the surface normal. Now, the value of the parameter V_T varies $T_o^{1/2}M^{-1/2}$, where T_o is the surface temperature and M is the particle mass [28]. Atomic mass number of Al, Ni, Mo, and Ta are 27, 59, 96, and 181, which shows a significant increase for the values of V_T for elements of lower atomic mass number. As a result, with increasing mass number, the thermal velocity V_T significantly decreases and there is a proportional increase in the parameter b, which results in pronounced focusing.

From Fig. 3 we note that the focusing effect increases as the charge state of the particles for any given focal spot size increases. This is much more clear for $B = 8.34\ mm^2$. The other focusing features that we find in Fig. 3 have already been discussed in the previous paragraphs. To explain this result, we have referred to the work of Sibold and Urbassek [11] in which, from a three-dimensional Monte Carlo study, they reported the formation of a desorption jet, in which fast particles are focused towards the jet axis, while slow particles leave the jet at oblique angles. In Fig. 4, we have the experimental results on average particle velocity as a function of the angle with the target normal for all the four elements. The results are displayed for four focal spot sizes. In each set, one can note that the ions with higher value of the charge state have larger average velocity. Therefore, the ions with higher values of the charge state are much more focused toward the target normal. Our experimental results clearly support the simulation results of Sibold and Urbassek [11].

In Table I, we have displayed the kinetic ion temperatures of Al, Ni, Mo, and Ta obtained from the time-of-flight spectra along the direction of target normal for representative two focal spot sizes of $B = 0.61$ and $8.34\ mm^2$. The corresponding laser intensities are also shown in the table. These kinetic temperatures result because of the complex interplay of absorption, recombination, and collision processes inside the plasma core. In general, one can say that the kinetic temperatures are lower for higher focal spot sizes, which is expected. They also further decrease with the increase in the atomic mass number. One can observe that ion temperatures are neither equilibrated among themselves nor with the electrons as the estimated spatially and temporally average electron temperatures of 71 ($B = 8.34\ mm^2$) and 85 eV ($B = 0.61\ mm^2$) are quite wide, off the estimated ion temperatures. This information can be useful in further analysis of the problem and investigations based on computer simulation.

IV. CONCLUSION

In the present work, we have investigated the direction-selective free expansion of laser plasma produced from planar, slab targets of Al, Ni, Mo, and Ta, using a 170 mJ, 5 nsec, Nd:YAG, Q-switched laser. All the experiments were performed at a fixed laser energy $E_L = 130$ mJ and different focal spot sizes varying from 0.61 mm^2 to 8.34 mm^2. Main experimental results are the following.

(1) For a given energy and the target element measurements of the particle, angular distribution showed that particles were more focused towards the target normal with increase in the values of B.

(2) For a given focal spot size B and the given energy, particle distribution was more focused towards the normal as

the atomic mass number of the target elements increased.

(3) For a given values of B and E_L, and for a given target element, the focusing effect towards the normal was more pronounced as the charge states of the ions increased.

These results have been fully explained on the basis of approximate calculations of recombination rates and particle collision frequencies and also on the basis of Monte Carlo simulations by Itina and co-workers [28,29] and Sibold and Urbassek [11]. These experimental results are in complete agreement with the computer simulations.

ACKNOWLEDGMENTS

The authors thank Franz Linder for helpful discussions and Hans Jürgen Feurich for technical support. One of us (B.K.S.) thanks Alexander von Humboldt Stiftung, Bonn, for financial support.

[1] R. K. Singh and J. Narayan, Phys. Rev. B **41**, 8843 (1990).
[2] D. K. Fork, J. B. Boyce, F. A. Ponee, R. I. Johnson, G. B. Anderson, G. A. N. Connell, C. B. Eom, and T. H. Geballe, Appl. Phys. Lett. **53**, 337 (1988).
[3] R. K. Singh, O. W. Holland, and J. Narayan, J. Appl. Phys. **68**, 233 (1990).
[4] R. Kelly, Nucl. Instrum. Methods Phys. Res. B **46**, 441 (1990).
[5] D. Sibold and H. M. Urbassek, Phys. Rev. A **43**, 6722 (1991).
[6] R. Kelly and B. Braren, Appl. Phys. B: Photophys. Laser Chem. **B53**, 160 (1991).
[7] K. Mann and K. Rohr, Laser Part. Beams **10**, 435 (1992).
[8] J. C. S. Kools, T. S. Baller, S. T. DeZwart, and J. Dieleman, J. Appl. Phys. **71**, 4547 (1992).
[9] R. Kelly, Phys. Rev. A **46**, 860 (1992).
[10] R. Kelly, A. Miotello, B. Braren, A. Gupta, and K. Casey, Nucl. Instrum. Methods Phys. Res. B **65**, 187 (1992).
[11] D. Sibold and H. M. Urbassek, J. Appl. Phys. **73**, 8544 (1993).
[12] H. M. Urbassek and D. Sibold, Phys. Rev. Lett. **70**, 1886 (1993).
[13] A. Thum, A. Rupp, and K. Rohr, J. Phys. D **27**, 1791 (1994).
[14] G. Granse, S. Völlmar, A. Lenk, A. Rupp, and K. Rohr, Appl. Surf. Sci. **96**, 97 (1996).
[15] S. I. Anisimov, D. Bäuerie, and B. S. Luk'yanchuk, Phys. Rev. B **48**, 12 076 (1993).
[16] R. Kelly and A. Miotello, Nucl. Instrum. Methods Phys. Res. B **91**, 682 (1994).
[17] E. Buttini, A. Thum-Jäger, and K. Rohr, J. Phys. D **31**, 2165 (1998).
[18] A. Thum-Jäger and K. Rohr, J. Phys. D **32**, 2827 (1999).
[19] T. Venkatesan, X. D. Wu, A. Inam, and J. B. Wachtmann, Appl. Phys. Lett. **52**, 1193 (1988).
[20] Th. Müller and Klaus Rohr, J. Phys. D **35**, 352 (2002).
[21] D. H. Lowendes, D. B. Geohegan, A. A. Puretaky, D. P. Norton, and C. M. Roulean, Surf. Sci. **273**, 898 (1996).
[22] R. Kelly and R. W. Dreyfus, Nucl. Instrum. Methods Phys. Res. B **32**, 341 (1988).
[23] R. Kelly and R. W. Dreyfus, Surf. Sci. **198**, 263 (1988).
[24] R. Kelly, J. Chem. Phys. **92**, 5047 (1990).
[25] I. Noor Batcha, R. R. Lucchese, and Y. Zeiri, J. Chem. Phys. **86**, 5816 (1987).
[26] I. Noor Batcha, R. R. Lucchese, and Y. Zeiri, Phys. Rev. B **36**, 4978 (1987).
[27] T. E. Itina, V. N. Tokarev, W. Marine, and M. Autric, J. Chem. Phys. **106**, 8905 (1997).
[28] T. E. Itina, W. Marine, and M. Autric, Appl. Surf. Sci. **127–129**, 171 (1998).
[29] B. K. Sinha and N. Gopi, Appl. Phys. Lett. **35**, 11 (1979).
[30] B. K. Sinha and N. Gopi, J. Appl. Phys. **51**, 1443 (1980).
[31] B. K. Sinha, N. Gopi, and S. K. Goel, Pramana **12**, 377 (1979).
[32] B. K. Sinha and N. Gopi, Phys. Fluids **23**, 1704 (1980).
[33] H. B. Kang, M. Waki, K. Yoshida, Y. Sakagami, T. Yamanaka, and C. Yamanaka, J. Phys. Soc. Jpn. **34**, 504 (1973).
[34] G. P. Enright, N. H. Burnett, and M. C. Richardson, Appl. Phys. Lett. **31**, 494 (1977).
[35] B. K. Sinha, J. Phys. D **13**, 1253 (1980).
[36] M. J. Bernstein and G. G. Comisar, J. Appl. Phys. **41**, 729 (1970).
[37] David Mosher, Phys. Rev. A **10**, 2330 (1974).
[38] G. P. Gupta and B. K. Sinha, J. Appl. Phys. **79**, 619 (1996).
[39] I. Kunz, Ph.D. thesis, Institut für Angewandte Physik, Technische Hochschule Darmstadt, 1990.
[40] L. Spitzer, *Physics of Ionized Gases* (Wiley, New York, 1962), p. 150.
[41] Ya. B. Zel'dovich and Yu. P. Raizer, *Physics of Shockwaves and High-Temperature Hydrodynamic Phenomena*, edited by W. D. Hayes and R. F. Probstein (Academic Press, New York, 1966), Vol. 1.
[42] F. F. Chen, *Introduction to Plasma Physics* (Plenum Press, New York, 1977), p. 352.
[43] A. Thum-Jäger, B. K. Sinha, and K. P. Rohr, Phys. Rev. E **63**, 061405 (2001).